Biofunctional and Tribo-mechanical Behavior of Porous Titanium Substrates Coated with a Bioactive Glass Bilayer (45S5 – 1393)

Ana M. Beltrán[a], Belén Begines[b], Ana Alcudia[b], José A. Rodríguez-Ortiz[a], Yadir Torres[a,*]

[a] Departamento de Ingeniería y Ciencia de los Materiales y el Transporte, Escuela Politécnica Superior, Universidad de Sevilla, Virgen de África 7, 41011 Seville, Spain

[b] Departamento de Química Orgánica y Farmacéutica, Facultad de Farmacia, Universidad de Sevilla, 41012 Seville, Spain

* Corresponding author: ytorres@us.es, phone: (+34) 954482276

Keywords: porous titanium substrates; bilayer coating; BG 45S5 and BG 1393; tribo-mechanical behavior; bioactivity.

Abstract

Porous substrates of commercially pure titanium have been coated with a novel bilayer of bioactive glasses, 45S5 and 1393, to improve the osseointegration and solve the stress-shielding phenomenon of titanium partial implants. The porosity of the substrates, the scratch resistance and bioactivity of the coating have been evaluated. Results are discussed in terms of stiffness and yield strength of the substrates, as well as the chemical composition, thickness and design of the bioglass coating (monolithic vs. bilayer). The role of the pores was a crucial issue in the anchoring of the coating, both in porosity percentage (30 and 60 vol. %) and pore range size (100 – 200 and 355 – 500 μm). The study was focused on the adhesion and infiltration of a 1393 bioglass layer (in contact with a porous titanium substrate), in combination with the biofunctionality of the 45S5 bioglass layer (surrounded by the host bone tissue), as 1393 bioglass enhances the adherence, while 45S5 bioglass promotes higher bioactivity. This bioactivity of the raw powder was initially estimated by nuclear magnetic resonance, through the evaluation of the chemical environments, and confirmed by the formation of hydroxyapatite, when immersed in simulated body fluid. Results revealed that

the substrate with 30 vol. % of porosity and a range of 355 – 500 μm pore size, coated with this novel bioactive glass bilayer, presented the best combination in terms of mechanical and biofunctional properties.

1. Introduction

Currently, life expectancy is increasing, thanks to the development of health care. However, living for more years implies the necessity of partial and/or total hard and soft tissue replacements as they can fail, due to many reasons, e.g., traumas, unhealthy lifestyles or, simply, their weakening. Considering this situation, it is necessary to find suitable materials to replace tissues. Among them, titanium is commonly used, due to its properties, such as high specific strength, low density, corrosion resistance and biocompatibility. However, it also presents drawbacks which limit its use in implants, such as the high Young´s modulus, compared to bone, which causes the stress-shielding phenomenon. In addition, micro-movements of implants have been associated with poor osseointegration of titanium, leading to implant loosening, and even failure [1–3]. To solve the first limitation, the use of porous materials is a good solution to minimize the problems associated with the Young´s modulus mismatch between the implant and the bone [4,5]. Different techniques to fabricate porous materials have been reported in the literature, such as powder metallurgy, foaming technologies and additive manufacturing methods [6–15]. Among all of them, the space-holder technique, based on powder metallurgy, is very promising, due to its versatility, reliability and low cost [16–20]. Nevertheless, pores (amount, size, morphology, inner roughness) can compromise the tribo-mechanical behavior (fracture, fatigue or wear), although they may allow infiltration of bone cells, as well as the adhesion of coatings. Concerning the poor osseointegration of the titanium implants, the use of bioactive coatings is widely used to stimulate bone generation. There are many types of coating (hydroxyapatites, biopolymers or bioactive glasses) and different techniques for their applications [21,22].

Independently of the coating or technique used, the lack of adherence to the implants and the bioactivity must be improved. Compared to other surface modifications, using bioactive materials, such as bioactive glass for coating metallic substrates, is more effective and efficient, due to their unique properties that could provide multiple functions [23]. Furthermore, they also present an extraordinary versatility based on the flexibility of their composition [24]. Therefore, focusing on bioactive glasses (BGs), they are a very versatile tool for biomedical application, from tissue regeneration to drug release [24]. The first definition of bioactive glass (BG) was given by Professor L. L. Hench, as special glasses able to bond to bone or even to soft tissues, without any rejection [25]. All of them have the ability to precipitate as hydroxyapatite (HA) on the glass surface, when they are in contact with physiological body fluid, allowing bonding to bone tissues. Chemically, the formed HA is very similar to that present in bones, which favors osseointegration of the implant [26]. Moreover, BGs also promote osteoinduction, involving the generation of new bone cells at the implant – bone interface [27]. Although the poor mechanical properties of BGs preclude their use as materials for implants, they fortunately behave well as coatings. An important factor is also surface roughness as it increases the bioactivity of the BGs. Higher HA production has been reported for nanotextured surfaces [28,29]. Hence, the control of BG porosity also implies control of the roughness and, therefore, the deposition technique has to be regulated since it would have an influence on the final texture.

The composition of the BG defines its properties [30]. There are several types, but they can be classified as silicate-, borated- and phosphate-based BG [31]. Among them, those silicate-based bioactive glass, and particularity, bioactive glasses 45S5 and 1393, have been widely used, thanks to their properties. On the one hand, BG 45S5 rapidly bonds to bone and stimulates bone growth away from the bone – implant interface, as well as presenting higher bioactivity than other BGs. The mechanism for bone bonding is attributed to the generation of an HA layer on the surface of the glass, induced by the BG [26]. On the other hand, BG 1393

presents a lower coefficient of thermal expansion (CTE), which is more similar to that of titanium, so it improves the adherence to the substrates [30]. However, its higher SiO_2 and MgO content implies a reduction in its bioactivity. Therefore, combining both BG 45S5 and BG 1393, is an interesting solution to gain the best characteristics of both.

The main aim of this manuscript is to present a potential, simultaneous solution to both the above mentioned problems of titanium (stress-shielding and poor osseointegration). Therefore, this research work proposes an implant based on the use of a novel BG bilayer coating (BG 45S5 and BG 1393) on porous substrates of commercially pure titanium (c.p. Ti), fabricated by the space-holder technique. In this case, the porosity of the substrates would be adequate to guarantee mechanical balance (stiffness and yield strength) and allow the infiltration of the coating and/or bone tissues. The BGs used were selected considering their properties. So, BG 1393 presents good adherence to the substrate (inner layer), thanks to its CTE which is more similar to that of c.p. Ti, while BG 45S5 has higher bioactivity and is located in contact with the bone tissue (outer layer). The bioactivity was measured through *in vitro* tests in simulated body fluid. In summary, this work presents an innovative design to overcome the limitations of the classical coated metal implants.

2. Materials and methods

C.p. Ti grade IV (according to ASTM: F67-13) with a particle size distribution $d_{[50]}$ = 23.3 μm [32], which was the median of the volume distribution, provided by SEJONG Materials Co. Ltd. (Seoul, Korea), was used for substrates. Ammonium bicarbonate (NH_4HCO_3), with a purity of 99 %, supplied by Cymit Química S.L. (Spain), was employed as the spacer.

The commercially available bioactive glasses BG 45S5 and BG 1393, were purchased from SCHOTT Vitrixx®. The chemical composition of BG 45S5 is 24.5 wt. % Na_2O, 24.5 wt. % CaO, 45 wt. % SiO_2 and 6 wt. % P_2O_5, while for BG 1393 it is 6 wt. % Na_2O, 12 wt. % K_2O,

5 wt. % MgO, 20 wt. % CaO, 53 wt. % SiO_2 and 4 wt. % P_2O_5 [31]. The BG 45S5 and BG 1393 powders present a $d_{[50]}$ of 4.5 and 6.1 μm, respectively, and both were received as the amorphous form.

To elucidate the strategy of choice when applying the bilayer coating, an estimation of the bioactivity of both BGs was performed. The HA formation from a BG layer occurs in five steps (Figure 1). Initially, an ion exchange takes place when Ca^{2+} and Na^{+} cations in the glass are substituted by H^{+} from the medium. This ionic interchange causes the breakage of the silicon network, inducing the formation of $Si(OH)_4$ in the BG surface. In a second step, silicic acid dissolves and repolymerizes, creating a convenient silica gel layer on the glass surface (third step). The fourth step consists of the incorporation of Ca^{2+} and PO_4^{3-} ions into the silica gel layer, which leads to the formation of an amorphous calcium phosphate surface layer. In a final step, HA crystalizes after the incorporation of CO_3^{2-} anions from the medium. Therefore, glass bioactivity is known to be related to its chemical structure and also to the particular silicon environments [33], and it is noted as (Q^n). These different environments depend on the number of non-bridging oxygens (NBO) that a silicon atom is bound to. In this sense, a Q^4 environment corresponds to a silicon atom linked to four (OSi) groups [$Si(OSi)_4$]. A Q^3 environment denotes a silicon atom bound to three (OSi) groups and an NBO [$(NBO)Si(OSi)_3$]. Likewise, Q^2 and Q^1 represent $(NBO)_2Si(OSi)_2$ and $(NBO)_3Si(OSi)_1$, respectively [34]. In general terms, a higher contribution of Q^2 and Q^3 environments is related to a greater bioactivity, as it means a more elevated number of NBO. Therefore, in order to evaluate the potential bioactivity of both BGs, the chemical structure of the silicon atoms in the tridimensional network was elucidated, conducting a ^{29}Si magic angle-spinning solid-state nuclear magnetic resonance (MAS NMR) study, prior to the deposition process. In this sense, raw BG samples were ground and introduced into the corresponding ^{29}Si MAS NMR rotor. The spectra were obtained using a Bruker Avance III 600 MHz WB spectrophotometer. Samples were spun at 10 kHz with a single pulse length of 75 º and a relaxation time of 15 s.

All chemical shifts were referenced to tetramethylsilane. Spectra deconvolution was performed using DMfit software.

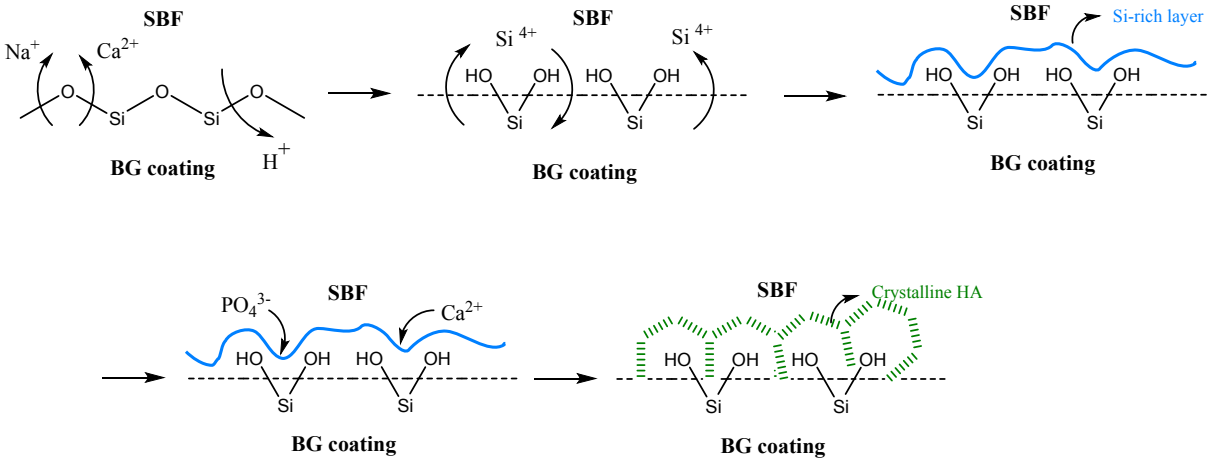

Figure 1: Schematic of the HA formation when the BG comes into contact with the SBF

2.1 Fabrication of porous c.p. Ti substrates

C.p. Ti substrates were fabricated by the space-holder technique, according to the procedure previously published by the authors [16,20,35,36]. In this study, four different substrates were manufactured, combining both the percentages (30 vol. % and 60 vol. %) and the size ranges (100 – 200 μm and 355 – 500 μm) of spacer particles. C.p. Ti powder was mixed with the corresponding quantity of ammonium bicarbonate spacer particles of the desirable size range and pressed at 800 MPa in an Instron 5505 machine. The ammonium bicarbonate was later removed, prior to the sintering of the substrates in a ceramic tubular furnace (2 h at 1250 ºC and ~10^{-5} mbar). Discs of 12 mm diameter and 2 mm height were fabricated. Measurements were performed on the whole discs or those split in two (D-shaped samples). The surfaces of the discs, as well as the surfaces and cross-sections of the D-shaped samples, were carefully ground and polished to preserve the porosity fraction, size and morphology of the pores, as well as to analyze the infiltration and thickness of the coating.

Figure 2 summarizes the main fabrication steps of the coated porous c.p. Ti substrates and the coating with the bilayer glass, as well as the appearance of the substrate surfaces, before

coating and after applying a thermal treatment to the deposited bilayer, with macrographs of the substrates.

2.2 Bioactive coating deposition

The dripping sedimentation technique was employed to coat the porous titanium substrates with a bilayer of two commercially available BGs (BG 45S5 and BG 1393) [37,38]. In order to keep the two halves of the D-shaped samples together and obtain a more homogeneous coating, avoiding the loss of the BG-suspension by the edges of the discs, substrates were surrounded with a retractable polymer, specifically, a polyolefin heat shrink polymer. A suspension of each BG was prepared with 0.1 g of the powder per 10 ml of ethanol, and was strongly stirred with a rod in an ultrasonic bath for 15 min to avoid sedimentation. Deposition is performed in four stages, as two layers of each BG is deposited, always following the same methodology: deposition and 24 h drying at room temperature to evaporate the ethanol. The deposition of two layers of each BG guarantees that the substrate would be fully-coated. Therefore, two layers of BG 1393 were deposited onto the c.p. Ti substrates, followed by two layers of BG 45S5. The coated substrates then underwent a heat treatment in a Vita Vacumat 6000 M furnace, at 820 ºC for 5 s in 10^{-2} mbar vacuum, (see Figure 2). Finally, the bilayer coatings were checked with an optical microscope to evaluate the homogeneity and quality (chipping and / or macro-cracking).

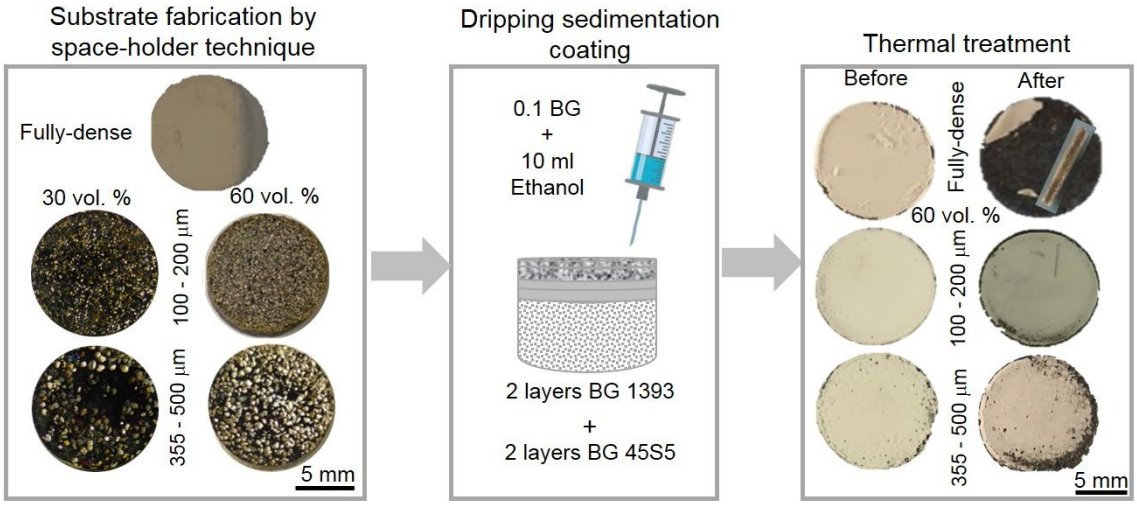

Figure 2: Scheme of the fabrication process of coated porous titanium substrates

2.3 Substrates and coating characterization

Before coating, the porous substrates were studied by image analysis (IA) to check that the volume and size of the pores agreed to fabrication conditions, i.e., the percentage and size range of the used spacer particles. The substrates were also evaluated by scanning electron microscopy (SEM) to obtain more information concerning the surface, as well as by energy-dispersive X-ray spectroscopy, coupled to the SEM (EDS-SEM) for compositional analyses with an FEI TENEO scanning microscope. These techniques were also used after coating to check details of the deposited BGs, such as the infiltration in the pores and the thickness of the bilayer coating, using the D-shaped samples to observe the substrate – BG 1393 – BG 45S5 interfaces. The infiltration was also determined on the D-shaped cut samples. Confocal laser microscopy (CLM) was also employed on the D-shaped samples to measure the surface roughness, specifically, parameters such as the arithmetical mean deviation (S_a), the root mean square height (S_q) and the maximum height (S_z), were determined.

Bioactive behavior of the bilayer coating

The bioactivity was evaluated through the immersion of all the coated samples (the whole cylinders), in simulated body fluid (SBF), during 21 days. The SBF was prepared following the protocol previously reported by Kokubo et al. [39]. It consists of dissolving 8.035 g · l^{-1} NaCl, 0.355 g · l^{-1} $NaHCO_3$, 0.225 g · l^{-1} KCl, 0.231 g · l^{-1} K_2HPO_4 ($3H_2O$), 0.311 g · l^{-1} $MgCl_2$ ($6H_2O$), 0.292 g l^{-1} $CaCl_2$, and 0.072 g · l^{-1} Na_2SO_4, in deionized water, and buffered at pH 7.4 at 36.5 °C with 6.118 g · l^{-1} tris(hydroxymethyl) aminomethane ($NH_2C(CH_2OH)_3$) and 1 M HCl. The samples were immersed in the SBF medium, inside a polystyrene container at 37 ºC, changing the suspension after 14 and 21 days to mimic *in vivo* behavior. After the incubation time, samples were washed with deionized water, dried and characterized, to

evaluate the formation of hydroxyapatite at the surface of the samples, after 14 and 21 days, by X-ray diffraction (XRD), conducted in a Bruker diffractometer D8 Advance A25 with a Cu Kα radiation of 0.154 nm, as well as by SEM micrographs, EDS-SEM and inductively coupled plasma atomic emission spectrometry (ICP).

In order to illustrate how the sintering affects the BG 45S5 in contact with the SBF, in terms of its chemical composition and, hence, its bioactivity, a ^{29}Si MAS NMR study should be conducted on the deposited and sintered material. However, the amount of material required to perform a MAS NMR experiment (100 mg approx.) is high, when compared to the amount of BG used for the coating. The very nature of the bilayer coating makes it extremely complicated to perform an adequate extraction of pure BG from the deposited coating, and much less feasible, considering the high amount required. Therefore, a piece of raw BG 45S5 sintered at 820 ºC was used to perform the ^{29}Si MAS NMR experiment. The modification of the bioactivity in BG 45S5, promoted by the temperature, will be discussed.

Tribological behavior of the bilayer coating

Scratch tests were performed to measure the scratch resistance of the coating, using a MICROTEST commercial device (MTR3/50-50/NI) with a Rockwell diamond tip of 200 μm diameter, and an incremental load from 0 to 3 N at a rate of 0.5 mm · min^{-1} for 3 mm of groove scar, following the standard ASRM C1624-05. These tests were performed on the surface of the samples, on the top-view of the cylinders.

The normal load was continuously recorded during scratching. Results were given as scratch penetration – load curves. At least three scratch tests were performed on each sample. Before the scratch test, samples were scanned to evaluate the roughness profile of the surface. From this test, different roughness parameters were determined: the arithmetic average of the absolute values of all points of the profile (R_a), the root mean square of the values of all points of the profile (R_q), the maximum peak-to-valley height of the entire measurement trace (R_y)

and the arithmetic average of the maximum peak-to-valley height of the roughness values of five consecutive sampling sections over the filtered profile (R_z).

The relationship between penetration depth, applied load and path, during the *in situ* scratch, was continuously recorded. Next, the real penetration depth of the groove scar (permanent deformation) was evaluated, as well as the roughness of the groove surface (this could vary, due to the presence of remaining BG resulting from the damage caused by scratch stresses), and an estimation of the elastic recovery of the coating. Finally, the micro-scratch scars were examined using a light microscope, along the whole scratch length, to discern the contact damage feature. One of the aims of this study is to evaluate the type of damage (chipping, cracking, etc.), generated in the bilayer coating, together with the applied threshold load in each case.

3. Results and discussion

This section has been divided into sub-sections according to the different aspects evaluated in this work. Firstly, details of the bioactivity of the BGs powders used for the coating are presented. Then, the microstructural and mechanical characterization of the porous titanium substrates is indicated and, finally, the degree of infiltration of the coating, its bioactivity and scratch resistance, are evaluated.

3.1 Characterization of the starting BGs powder

Firstly, the BGs were characterized to evaluate their bioactivity and corroborate the use of the selected BG 45S5 and BG 1393. To establish an optimal strategy for the bilayer formation, the potential bioactivity of both BGs was considered as the key factor. To determine the ideal candidate to be in contact with the SBF, a chemical characterization was performed using ^{29}Si MAS NMR, in both BG 45S5 and BG 1393, as raw powder materials. As was described above, the glass that presents higher contribution of Q^2 and Q^3 environments should possess

an enhanced bioactivity. Therefore, the BG containing a more significant contribution of these environments would be the one deposited on top and, hence, in contact with the SBF. Figure 3 displays the results obtained from the ^{29}Si MAS NMR for both BGs. Particularly, raw BG 45S5 clearly presented a strong influence of Q^2 and Q^3 environments, with chemical shifts appearing at approximately -80 and -87 ppm, respectively, slightly shifting to a lower field of the spectrum, if compared to usual values previously described in the literature for other BGs [40,41]. However, BG 1393 displayed a signal with major contributions of Q^4 and Q^3 environments, appearing at -110 ppm and -100 ppm, respectively. These chemical shift displacements, placed in the high field of the NMR spectrum, correspond to a silicon network with a more elevated polymerization level. The signal deconvolution was carried out for both BGs. As displayed in Table 1, raw BG 1393 possessed a 45 % contribution of the Q^4 environment, while the contribution corresponding to the Q^3 environment was equivalent to 55 % of the total signal. This experiment suggested that the participation of the Q^2 environment in the raw BG 1393 was irrelevant. However, the contributions for BG 45S5 were 35 % and 65 % for Q^3 and Q^2 environments, respectively. In this case, the irrelevant participation corresponds to the Q^4 environment, indicating an extremely low silicon polymerization, a high number of NBO and, therefore, a more significant bioactivity. These results point to BG 45S5 as the more convenient BG to be in contact with the SBF, as it could generate HA on its surface more effectively than BG 1393.

Table 1: Contribution in % of the different environments to each BG

Bioglasses	**Q^n environments (%)**		
	Q^2	Q^3	Q^4
1393 before sintering	-	55	45
45S5 before sintering	65	35	-

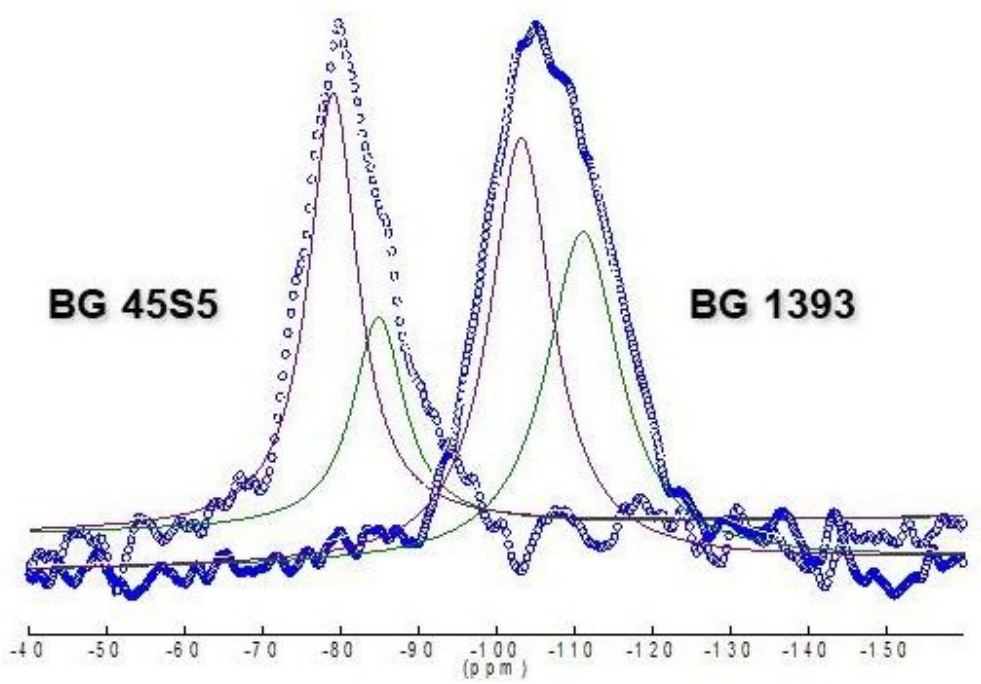

Figure 3: ^{29}Si MAS NMR of BG 45S5 and BG 1393 and their corresponding deconvolution curves

3.2 Characterization of the porous c.p. Ti substrates

Since the evaluation of the biomechanical and biofunctional balance was carried out as a function of the percentage of porosity and pore size, it was crucial to evaluate these characteristics in all the uncoated porous c.p. Ti substrates, as well as their mechanical properties, which were estimated from the total and interconnected porosity of the substrates. Then, all the fabricated substrates were fully characterized in order to confirm the formation of the desirable porosity, according to the size and volume of the used spacer particles. The mechanical behavior of the porous substrates (dynamic Young´s modulus, E_d, yield strength, σ_y), were estimated using the equations reported in the literature [42]. The microstructural parameters used for such estimations were: total porosity, P_T, and interconnected porosity, P_i, determined by Archimedes' method, already reported in other works [38,42,43]. All the results were summarized in Table 2, where a decrease of the Young´s modulus can be

observed, as the size and percentage of porosity increase, being more similar to the natural bone [3].

Table 2. Mechanical properties estimated from porosity values

	P_i (%)	P_T (%)	E_d (GPa)	σ_y (MPa)
30 vol. %, 100 – 200 μm	19.7	32.7	53.9	334.7
30 vol. %, 355 – 500 μm	25.6	33.9	52.54	259.8
60 vol. %, 100 – 200 μm	51.8	56.4	32.3	84.2
60 vol. %, 355 – 500 μm	53.0	57.78	31.4	80.1

3.3 Microstructural characterization of the cross-section of the bilayer coated c.p. Ti substrates

Once the mechanical properties of the uncoated porous c.p. Ti substrates were analyzed, they were coated (the full-cylinder or in the D-shaped form) and characterized to evaluate the thickness and homogeneity. These studies were performed on the D-shaped samples, as the cross-sectional view allows the interfaces between the Ti – BG 1393 – BG 45S5 layers to be observed. As an example, Figure 4a displays a SEM micrograph of a cross-section of the 30 vol. %, 100 – 200 μm c.p. Ti porous substrate, and the bilayer coating on the c.p. Ti substrate, and the infiltration into the pores, can be observed. From such images, the thickness of the BG layers was measured, revealing that BG 45S5 was thinner than BG 1393 (27.4 ± 8.2 μm vs. 62.3 ± 3.6 μm, respectively). In the case of the CLM images (Figure 4b), details about the roughness of the studied area of the D-shaped samples were shown. Roughness inside the pores could also be seen in Figure 3a. From these images, it was confirmed that the BG 45S5 layer presents a microporous structure, which would contribute to promoting its interaction with the bone tissues. It was also observable that BG 1393 displayed a typical vitreous appearance (dense and transparent) with the presence of small bubbles. Previous studies by the authors of this work have already reported the roughness of the pore walls, and how it enhances the adherence of the coating, as is displayed in Figure 3b [38].

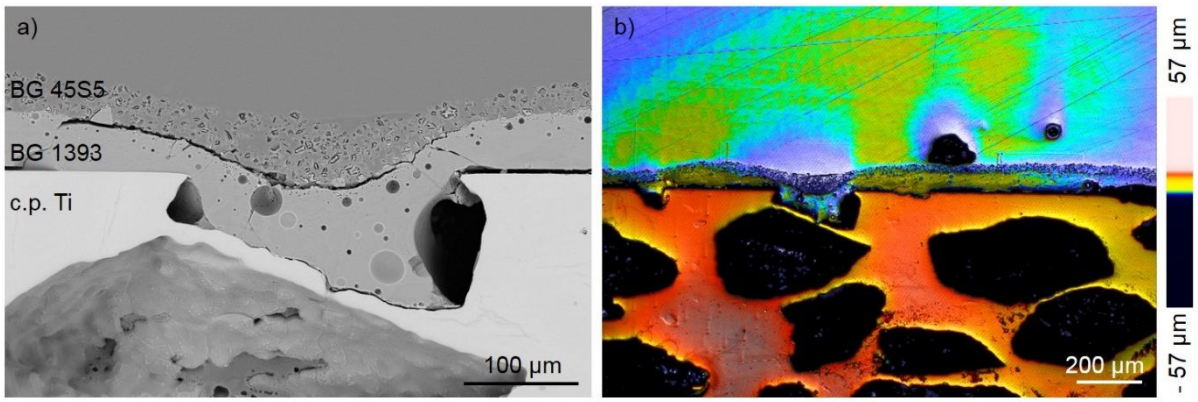

Figure 4: Cross-section a) SEM micrograph and b) CLM image of the 30 vol. %, 100 – 200 µm sample

3.4 Biofunctional behavior of the bilayer coating

After analyzing the porosity and biomechanical behavior, the next step was the evaluation of the bioactivity, once the substrates were coated with the BG 45S5 – BG 1393 bilayer. Apart from the bilayer coated porous substrates, additional samples were studied as references (i.e., fully-dense substrate and porous substrates coated with just one type of BG, which was named monolithic BG coating). These experiments were performed on the whole cylindrical samples. The bioactivity of the coated samples was measured as a function of the HA formation after 21 days in SBF, taking the Ca / P ratio as a reference, which is estimated to be 1.67 in natural HA [44]. As was mentioned, SBF tests were performed not only on the bilayer coated samples (BG 45S5 – BG 1393), i.e., the four analyzed substrates (30 vol. %, 100 – 200 µm; 30 vol. %, 355 – 500 µm; 60 vol. %, 100 – 200 µm; 60 vol. %, 355 – 500 µm), but also on all the substrates coated with just one BG: monolithic coating BG 45S5 or monolithic coating BG 1393. Furthermore, a fully-dense sample was also studied as a reference. The morphology, phases and chemical composition of the material formed on the surface was later analyzed, at 14 and 21 days, using different techniques.

Figure 5 displays SEM images of the surface of the coated c.p. Ti substrates before, and after, 21 days of immersion in SBF. The observed morphology is typical of calcium phosphates present in bone tissues, and this was corroborated by different analytical techniques. XRD

analyses (Figure 6) revealed a Ca / P ratio typical of HA. ICP results also showed a right Ca / P balance, between the SBF composition, and the compound formed on the surface of the bilayer coated substrates (Table 3). Likewise, EDS-SEM revealed similar conclusions (Table 4). Results were compared to fully-dense samples, although this type of substrate was not deeply investigated in this work, as it was only a reference sample. Tables 3 and 4 also show the analyses after 14 days of immersion in SBF. Despite an increase of Si content being observed at this time, it was related to a partial solution of the BG during the formation of the silica gel layer in the BG – SBF interface [45]. Then, after 21 days, Si content decreased for both BGs, as the SBF was renewed and the amount of remaining BG was reduced, so after 21 days, it could be confirmed that the BGs were stabilized. It was also remarkable to take into account that the release and balance of Si must be considered, because it promotes the formation and proliferation of osteoblasts, but inhibits the induction process and the growth of osteoclasts [46].

Comparing the monolithic BG 45S5 and bilayer coatings, XRD patterns did not show the characteristic peaks of the $Na_2Ca_2Si_3O_9$ phases, however, the presence of rutile (TiO_2) and compounds, typically associated with HA, were detected (Figure 6), in accordance with results reported in the literature [47,48]. Comparing the chemical analyses of SBF after 21 days, they all revealed that the Ca / P ratio was quite similar to natural HA.

BG bilayer coatings were compared to the monolithic BG, and the Ca / P ratio from BG 45S5 was more similar to natural HA, than that from BG 1393 (Table 4), as could be expected. Also, the morphological similarities were clear (Figure 7), this being attributable to the higher bioactivity of BG 45S5 (better osseointegration).

In view of the results obtained after immersion in SBF, it could be said that the c.p. Ti substrates with a 30 vol. % in porosity presented better bioactivity, as the Ca / P ratio is more similar to that of natural HA.

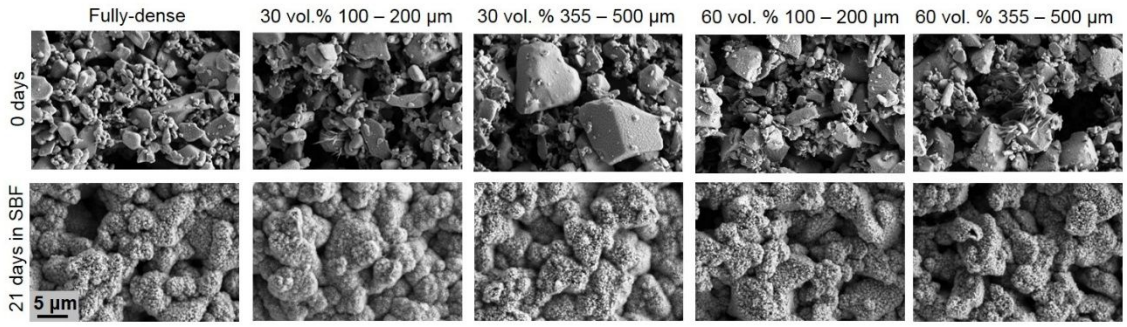

Figure 5: SEM micrograph of the different substrates studied, before and after 21 days immersion in SBF. Common scale bar

Table 3. Variation of the chemical composition of the SBF by ICP. Influence of the bilayer coating on the formation of HA (Ca / P ratio)

Days	0		14					21			
($mg \cdot l^{-1}$)	SBF	Fully-dense	30 %		60 %		Fully-dense	30 %		60 %	
			100-200	355-500	100-200	355-500		100-200	355-500	100-200	355-500
Ca	74.3	62.4	65.4	68.8	64.8	66.2	61.0	59.2	66.1	60.3	65.0
P	39.2	10.7	11.4	13.7	9.4	10.7	25.5	24.2	27.3	21.1	23.7
Si	≤ 0.041	49.5	49.1	49.9	53.9	49.5	10.8	13.9	11.2	23.1	9.54
Ti	≤ 0.004			≤ 0.002					≤ 0.010		
Ca / P atomic	1.46	4.08	4.44	3.88	5.33	4.78	1.85	1.89	1.87	2.21	2.12
% Discrepancy	1.80	144.1	166.1	132.3	219.1	186.4	10.6	13.2	12.1	32.2	27.0

Note: Discrepancy calculated with respect to the Ca / P ratio of natural HA, 1.67 [44]

Table 4. Chemical composition of the surface of the coated substrates after 21 days in SBF of the monolithic and bilayer coatings by EDS-SEM

		BG 1393				Bilayer				BG 45S5			
At. %	Fully-dense	30 vol. %		60 vol. %		30 vol. %		60 vol. %		30 vol. %		60 vol. %	
		100-200	355-500	100-200	355-500	100-200	355-500	100-200	355-500	100-200	355-500	100-200	355-500
Ca	61.21	6.29	9.07	56.14	40.00	60.52	35.84	61.9	60.09	31.99	60.94	61.38	58.10
P	38.12	2.92	8.85	39.99	25.71	39.16	21.28	37.17	39.34	16.79	39.06	37.38	41.11
Si	0.67	57.57	82.08	3.86	34.29	0.32	0.05	1.75	0.57	0.03	≤ 0.002	1.24	0.78
Ca/P atomic	1.61	2.16	1.02	1.40	1.56	1.55	1.68	1.64	1.53	1.91	1.56	1.64	1.41
% Discrepancy	3.6	29.3	38.9	16.2	6.6	7.2	0.6	1.8	8.4	14.4	6.6	1.8	15.6

Note: Discrepancy calculated with respect to the Ca / P ratio of natural HA, 1.67 [44]

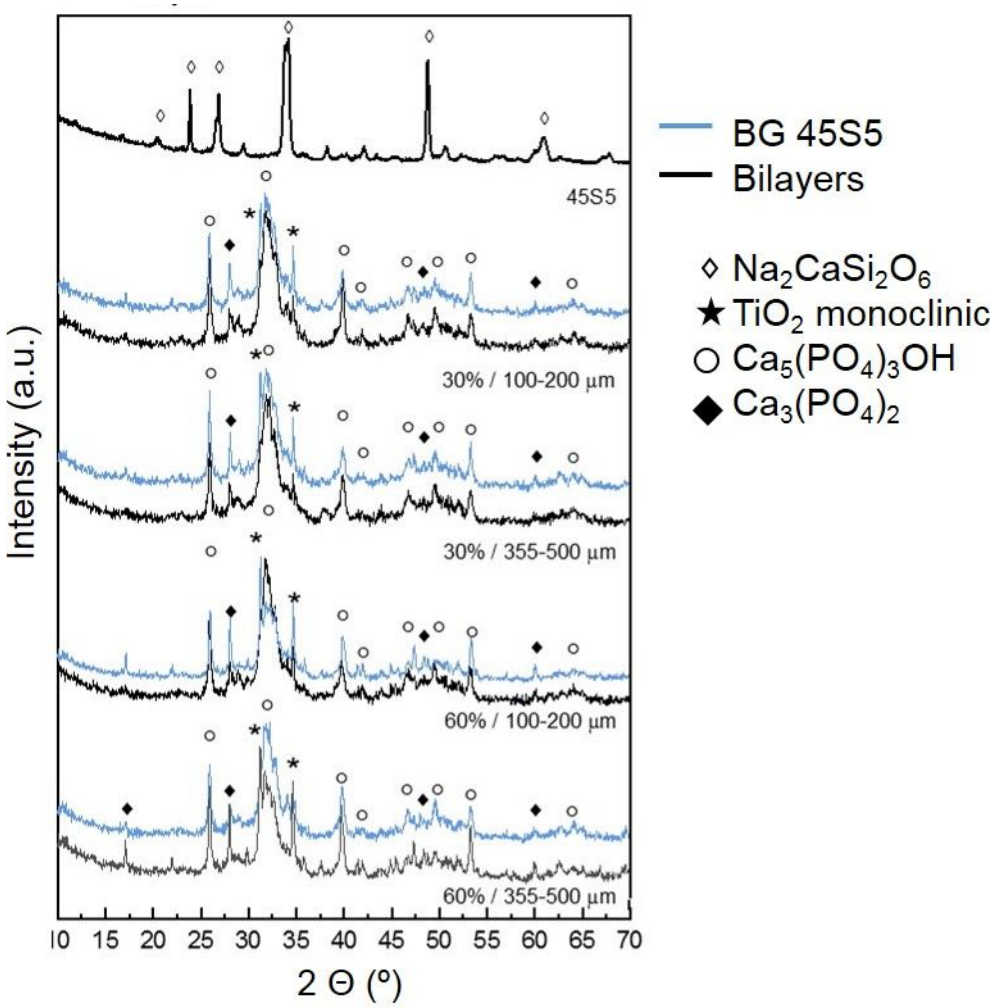

Figure 6: XRD patterns of the BG 45S5 monolithic and bilayer coatings after 21 days immersion in SBF

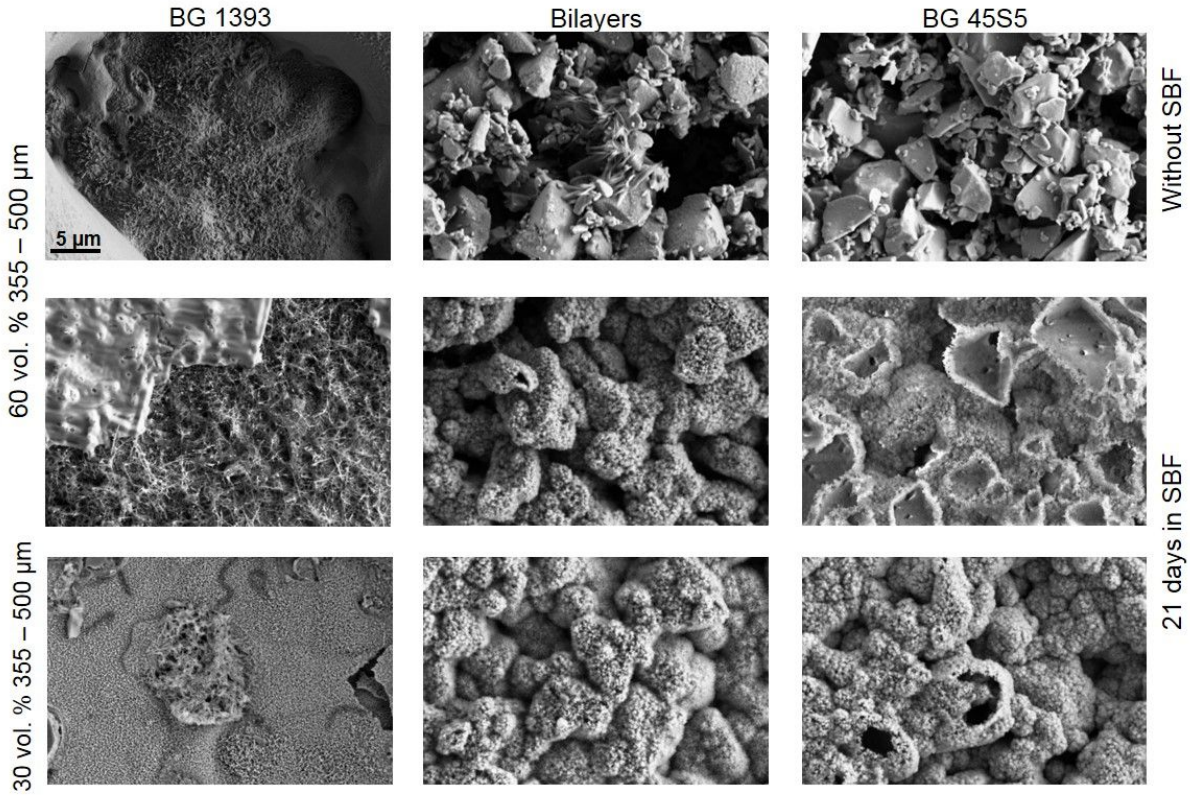

Figure 7: SEM micrograph of the different studied substrates with higher pores size compared to the BGs, before and after 21 days in SBF. Common scale bar

Although generation on top of the bilayer has been proved, an estimation on how the sintering process could have affected the bioactivity of BG 45S5 was conducted. In this sense, the ^{29}Si MAS NMR spectrum, previously obtained for the raw glass, was compared with the spectrum acquired from a ground sample of the same BG, but sintered at 820 ºC. Figure 8 shows the results of the MAS NMR experiments performed on BG 45S5, before, and after, sintering. In general terms, a clear displacement to the right (higher field of the spectrum) was observed after the temperature treatment. While the raw glass exhibited a greater contribution of Q^2 and Q^3 environments, as previously described, the sintering process promoted a signal movement, indicating more participation of Q^3 and Q^4 environments, with peaks centered at -101 ppm for Q^3 and -110 ppm for Q^4. A small contribution of Q^2 could also be appreciated, centered at -91 ppm. The total contribution of each environment was summarized in Table 5, where it

could be observed that the Q^4 environment contributed 54 % to the total signal, while Q^3 participated with 44 %. The remaining 2 % was associated with a Q^2 environment. These results demonstrated that the sintering process causes a reduction in the BG bioactivity, probably due to an increment in the polymerization of silicon atoms, and the consequent decrease in the number of the NBO, inducers of HA formation.

Table 5: Contribution in % of the different environments to BG 45S5

Bioglass	**Q^n environments (%)**		
	Q^2	Q^3	Q^4
BG 45S5 before sintering	65	35	-
BG 45S5 after sintering	2	44	54

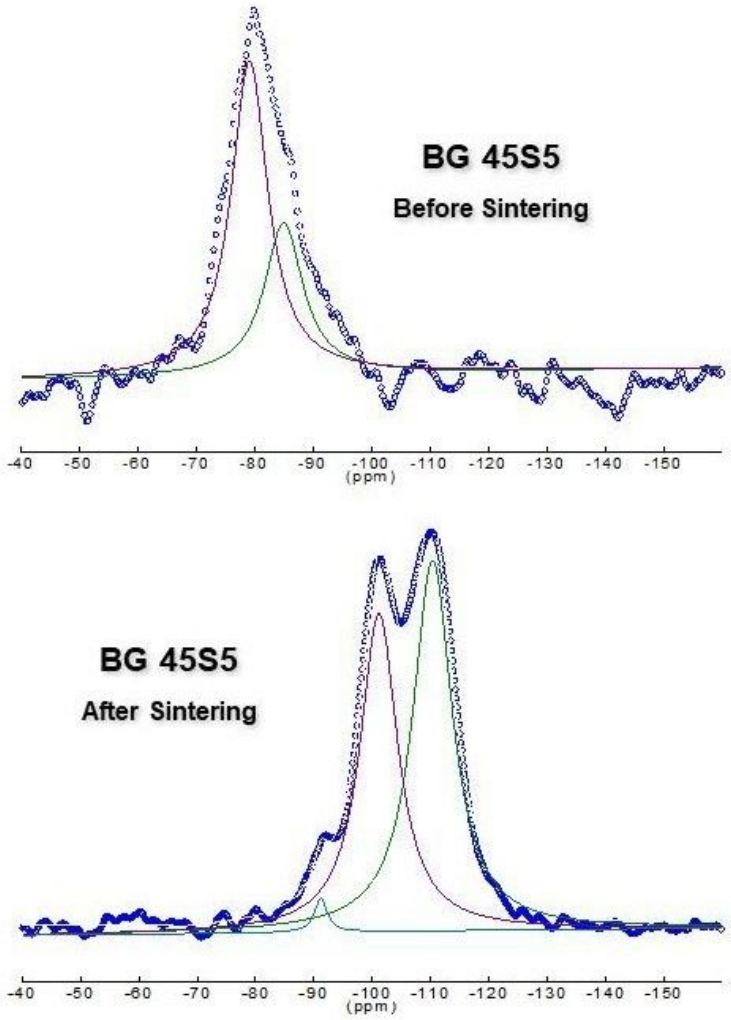

Figure 8: ^{29}Si MAS NMR spectra of BG 45S5 before, and after, sintering. Both spectra include the components of each signal deconvolution

The MAS NMR measurements, and the results of *in vitro* studies in SBF presented in this work, suggest a potential osseointegration capacity of the proposed coated implants. New experiments concerning *in vivo* tests are planned to be conducted, in the near future, to elucidate the suitability of this novel implant design. In this context, the expected behavior of the proposed bilayer coating is promising, taking other works already published, related to this behavior of a biomedical implant, as a reference [23,24,49–51].

3.5 Scratch resistance of the coatings

After analyzing the mechanical properties of all the uncoated porous c.p. Ti substrates, it was observed that the 30 vol. %, 100 – 200 μm sample showed Young´s modulus, and a yield strength performance, that was more similar to natural bone. Thus, biocompatibility studies by immersion in SBF also pointed to the 30 vol. % porosity substrates (and both pore sizes) as the most adequate. Hence, to continue the characterization, scratch tests were performed for a better understanding of the mechanical behavior, through tribomechanical analyses with the coated substrates at 30 vol. % porosity, and at the two different, previously studied, pore sizes. Measures were focused on evaluating the scratch resistance of the deposited coatings (BG 45S5 monolithic vs. bilayer) on such substrate. As mentioned above, before performing the scratch test, the surface roughness of the coating where the scratch resistance measurement would be carried out was evaluated. This information is summarized in Table 6. There was a direct relationship between the characteristics of the porosity of the c.p. Ti substrates and the roughness of the coating, as it mimics the surface of the sample, and even the pores, due to the infiltration, as was shown in Figure 4.

Table 6: Surface roughness parameters of the studied samples
Relative error below 0.1%

	Pore size (μm)	R_a (μm)	R_q (μm)	R_z (μm)	R_y (μm)
30 vol. %	100 – 200	5.6	2.4	20.5	20.5
	355 – 500	17.4	4.2	49.5	49.5
60 vol. %	100 – 200	4.1	2.0	11.9	11.9
	355 – 500	30.4	5.5	46.9	47.0

Figure 9 shows the variation of the penetration depth when the incremental load was applied, evaluating the influence of the coating composition (BG 45S5 monolithic vs. BG 45S5 – BG 1393 bilayer) and the pore size of the c.p. Ti substrate. The penetration depth would provide a measure of the resistance to penetration of the coating. The optical images, included in Figure 9, were acquired in areas of the scratch groove that correspond to the applied load values where representative changes in the trends of the penetration depth curves were detected. Table 7 summarizes these data for maximum penetration depth and elastic recovery at the above-mentioned condition. The analysis of the results obtained from the graphics (Figure 9), and parameters of Table 7, allow several aspects to be highlighted. On the one hand, for the same volume of c.p. Ti substrate porosity (30 vol. %, 100 – 200 μm vs. 355 – 500 μm), and independently of the type of coating (monolithic BG 45S5 or bilayer), the scratch resistance decreases (higher penetration depth) as the pore size increases. This result may be related to the lower rigidity and mechanical resistance of this substrate (355 – 500 μm). In this context, when the pore size increases, scratch resistance decreases approximately 94 % in monolithic BG 45S5 coating, and 226 % for the bilayer coating. On the other hand, concerning the influence of the type of coating (monolithic BG 45S5 or bilayer), changes were observed in the penetration depth trend as it firstly increases, and then, decreases. These changes may be associated with the interface between coating and substrate and between BG 45S5 – BG 1393. In general, these observed trends in the behavior of coatings were consistent with the characteristics of the tested coatings: BG 45S5 was

microporous (lower hardness), while BG 1393 showed a behavior similar to a dense glass (higher hardness and brittleness). It could also be observed that, regardless of the type of porous c.p. Ti substrate, the scratch resistance of the bilayer coated samples was higher than those coated with monolithic BG 45S5. Thus, increases are observed for the bilayer of 73 % (substrates of 100-200 μm) and 56 % (substrates with the larger pores). The red vertical dashed lines of Figure 9a and 9b represent when these changes in the trends of penetration depth occurred for each applied load. It can be appreciated that the scratch resistance of the bilayer coatings was higher than that of the monolithic BG 45S5. As an example, in the bilayer coatings, this change (see the dashed line) occurred for applied loads of 0.65 N (100 – 200 μm) and 1.85 N (355 – 500 μm). The change from light to dark tone of the groove is remarkable (optical image Figure 9c). In this context, considering the appearance after the heat treatment of BG 45S5 (off-white) and BG 1393 (dark gray), it could be corroborated that the transition within the bilayer glass occurred in that area. In addition, these changes in the penetration depth also allow estimation of the thickness of the (monolithic) BG 45S5 layer (~ 28 μm), as a sharp decrease in the curves was observed when contacting the c.p. Ti substrate (harder). However, it was not possible to discriminate the thicknesses in the bilayer as it required other more suitable techniques, such as SEM or CLM, to be performed on the cross-section of the samples. Also, it is noticeable how the elastic recovery values of the bilayer were higher, up to the transition (BG 1393 layer, with ceramic behavior) and lower after the transition, and until the end of the measurement (the c.p. Ti substrates with metallic behavior), while the microporous coatings of the monolithic BG 45S5 experienced intermediate elastic recovery values.

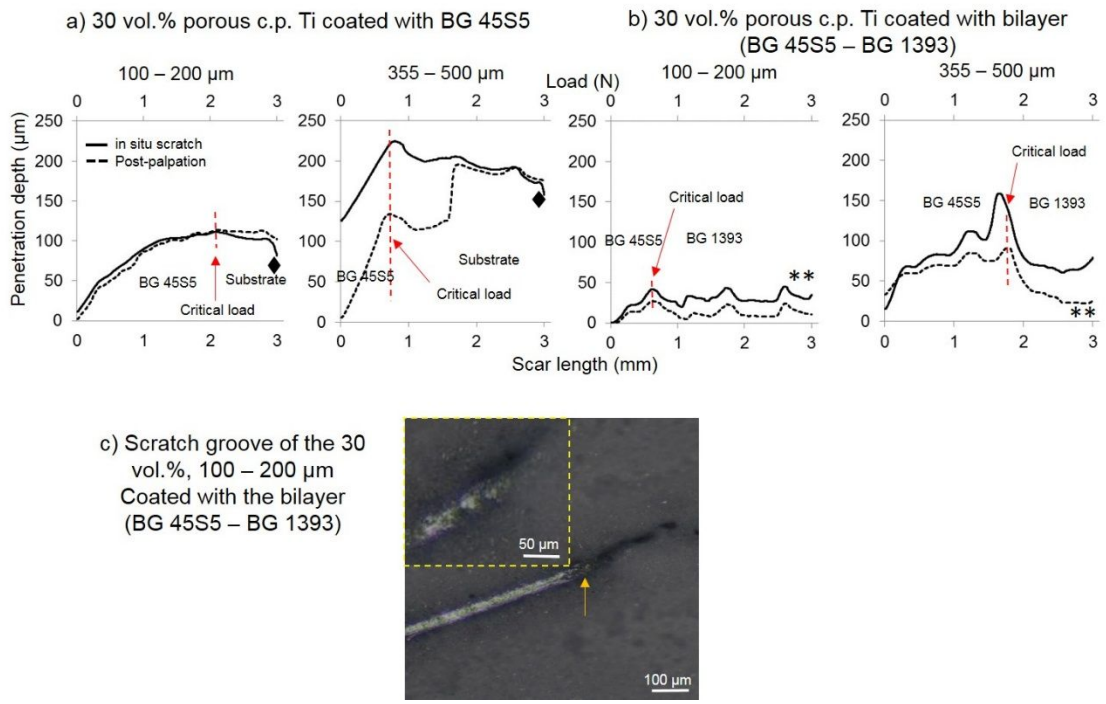

Figure 9: Scratch resistance (increasing load from 0 to 3 N) for the coated substrates: a) monolithic BG 45S5; b) bilayer coating. Influence of the applied load, type of coating and pore size; c) Optical image of the scratch groove in the bilayer coated substrate. The arrow indicates the change from white to black

Note: The symbols (♦ and **) and red dashed lines (- - -) are explained in Table 7

Table 7. Penetration depth and elastic recovery of the 30 vol. % Ti porous substrates. Reference: applied load associated to a change of the trend

		Left of the reference		**Right of the reference**	
		MAX. penetration depth (μm) ~ (thickness of BG 45S5)	Average elastic recovery (%)	MIN. penetration depth (μm) (μm) ~ ♦ Scratch resistance of the substrate or ** BG 1393 (max. load = 3 N)	Average elastic recovery (%)
BG 45S5 monolithic – 30 vol.%	100 – 200 μm	101	15	100♦	0
	355 – 500 μm	196	47	176♦	1
Bilayer – 30 vol. %	100 – 200 μm	27	36	5**	58
	355 – 500 μm	88	19	22**	51

Note: Left and right refer to the side of the transition, dashed lines, refer to the curves of Figure 9.

4. Conclusions

In summary, this work presents results of bioactivity and tribo-mechanical evaluation of c.p. Ti substrates, fabricated by the space-holder technique, coated with a novel BG 45S5 and BG 1393 bilayer, deposited by a simple and low-cost technique: dripping-sedimentation. Two ranges of pore size were studied, 100 – 200 and 355 – 500 μm, and two percentages of porosity, 30 and 60 vol. %. The criterion to select this combination of BGs was corroborated by MAS NMR, and it confirmed that BG 45S5 was the most suitable BG to be in contact with the SBF, as it could more effectively generate HA on its surface than BG 1393. In fact, this

bilayer coating showed an enhanced bioactivity, evaluated by the formation of superficial compounds with a Ca / P ratio similar to natural hydroxyapatite, induced by the BG 45S5 in contact with SBF, these results being even closer to natural HA (Ca/P ~ 1.67) for the 30 vol. % , 355 – 500 μm substrate. However, BG 1393 presents a similar CTE to titanium, which enhances adhesion to the substrate.

In terms of mechanical properties, among the different substrates investigated, the combination of 30 vol. % of porosity of a pore size range of 355 – 500 μm revealed the best results in terms of tribo-mechanical properties.

In summary, the 30 vol. % and 355 – 500 μm pore size substrate coated with the novel bilayer design, BG 45S5 – BG 1393, is a very suitable combination for implants, achieving an adequate biomechanical and biofunctional balance.

Acknowledgments

This work was supported by the Junta de Andalucía–FEDER (Spain), through the Project Ref. US-1259771, and the Project 2004/00001203 (RYC-2004-001497), from M.C.E. (Spain). The authors would also like to thank students, J.A. Guardiola and P. Lechuga, for their contribution, Laboratory Technician, J. Pinto, for his support in the scratch tests, the University of Seville Research, Technology and Innovation Centre (CITIUS) (NMR, SEM, ICP, XRD), and Dr. M. Dolores Alba, for her very useful discussions.

References

[1] L. Kunčická, R. Kocich, T.C. Lowe, Advances in Metals and Alloys for Joint Replacement, Prog. Mater. Sci. 88 (2017) 232–280. https://doi.org/10.1016/j.pmatsci.2017.04.002.

[2] K. Pałka, R. Pokrowiecki, Porous Titanium Implants: A Review, Adv. Eng. Mater. 20 (2018) 1700648 (1–18). https://doi.org/10.1002/adem.201700648.

[3] M. Kaur, K. Singh, Review on Titanium and Titanium Based Alloys as Biomaterials for Orthopaedic Applications, Mater. Sci. Eng. C. 102 (2019) 844–862. https://doi.org/10.1016/j.msec.2019.04.064.

[4] X. Miao, D. Sun, Graded/Gradient Porous Biomaterials, Materials 3 (2010) 26–47. https://doi.org/10.3390/ma3010026.

[5] C. Betts, Benefits of Metal Foams and Developments in Modelling Techniques to Assess their Materials Behaviour: a Review, Mater. Sci. Technol. 28 (2012) 129–143. https://doi.org/10.1179/026708311X13135950699290.

[6] I.H. Oh, N. Nomura, S. Hanada, Microstructures and Mechanical Properties of Porous Titanium Compacts Prepared by Powder Sintering, Mater. Trans. 43 (2002) 443–446. https://doi.org/10.2320/matertrans.43.443.

[7] G. Ryan, A. Pandit, D.P. Apatsidis, Fabrication Methods of Porous Metals for Use in Orthopaedic Applications, Biomaterials. 27 (2006) 2651–2670. https://doi.org/10.1016/j.biomaterials.2005.12.002.

[8] Y.J. Chen, B. Feng, Y.P. Zhu, J. Weng, J.X. Wang, X. Lu, Fabrication of Porous Titanium Implants with Biomechanical Compatibility, Mater. Lett. 63 (2009) 2659–2661. https://doi.org/10.1016/j.matlet.2009.09.029.

[9] Y. Xiong, C. Qian, J. Sun, Fabrication of Porous Titanium Implants by Three-Dimensional Printing and Sintering at Different Temperatures, Dent. Mater. J. 31 (2012) 815–820. https://doi.org/10.4012/dmj.2012-065.

[10] M. Naebe, K. Shirvanimoghaddam, Functionally Graded Materials: A Review of Fabrication and Properties, Appl. Mater. Today. 5 (2016) 223–245.

https://doi.org/10.1016/j.apmt.2016.10.001.

[11] X.P. Tan, Y.J. Tan, C.S.L. Chow, S.B. Tor, W.Y. Yeong, Metallic Powder-Bed Based 3D Printing of Cellular Scaffolds for Orthopaedic Implants: A State-of-the-Art Review on Manufacturing, Topological Design, Mechanical Properties and Biocompatibility, Mater. Sci. Eng. C. 76 (2017) 1328–1343. https://doi.org/10.1016/j.msec.2017.02.094.

[12] S. Singh, S. Ramakrishna, R. Singh, Material Issues in Additive Manufacturing: A Review, J. Manuf. Process. 25 (2017) 185–200. https://doi.org/10.1016/j.jmapro.2016.11.006.

[13] C. Chen, Y. Hao, X. Bai, J. Ni, S.M. Chung, F. Liu, I.S. Lee, 3D Printed Porous Ti6Al4V Cage: Effects of Additive Angle on Surface Properties and Biocompatibility; Bone Ingrowth in Beagle Tibia Model, Mater. Des. 175 (2019) 107824. https://doi.org/10.1016/j.matdes.2019.107824.

[14] R. Kobatake, K. Doi, T. Kubo, Y. Makihara, Y. Oki, M. Yokoi, H. Umehara, K. Tsuga, Novel Fabrication of Porous Titanium by a Resin-Impregnated Titanium Substitution Technique for Bone Reconstruction, RSC Adv. 9 (2019) 1625–1631. https://doi.org/10.1039/C8RA08744J.

[15] H.J. Yun, D. Abolhasani, T.W. Hwang, T. Lee, J.H. Kim, Y.H. Moon, Fabrication of Porous Titanium Parts by Powder Bed Fusion of Ti-TiH_2 Blended Powder, J. Mater. Res. Technol. (2020) 1–12. https://doi.org/10.1016/j.jmrt.2020.01.033.

[16] Y. Torres, J.A. Rodríguez, S. Arias, M. Echeverry, S. Robledo, V. Amigo, J.J. Pavón, Processing, Characterization and Biological Testing of Porous Titanium Obtained by Space-Holder Technique, J. Mater. Sci. 47 (2012) 6565–6576. https://doi.org/10.1007/s10853-012-6586-9.

[17] Y. Torres, J.J. Pavón, J.A. Rodríguez, Processing and Characterization of Porous Titanium for Implants by Using NaCl as Space Holder, J. Mater. Process. Technol. 212

(2012) 1061–1069. https://doi.org/10.1016/j.jmatprotec.2011.12.015.

[18] D.P. Mondal, M. Patel, S. Das, A.K. Jha, H. Jain, G. Gupta, S.B. Arya, Titanium Foam with Coarser Cell Size and Wide Range of Porosity Using Different Types of Evaporative Space Holders Through Powder Metallurgy Route, Mater. Des. 63 (2014) 89–99. https://doi.org/10.1016/j.matdes.2014.05.054.

[19] J. Jia, A.R. Siddiq, A.R. Kennedy, Porous Titanium Manufactured by a Novel Powder Tapping Method Using Spherical Salt Bead Space Holders: Characterisation and Mechanical Properties, J. Mech. Behav. Biomed. Mater. 48 (2015) 229–240. https://doi.org/10.1016/j.jmbbm.2015.04.018.

[20] S. Muñoz, J. Pavón, J.A. Rodríguez-Ortiz, A. Civantos, J.P. Allain, Y. Torres, On the Influence of Space Holder in the Development of Porous Titanium Implants: Mechanical, Computational and Biological Evaluation, Mater. Charact. 108 (2015) 68–78. https://doi.org/10.1016/j.matchar.2015.08.019.

[21] Y. Liu, B. Rath, M. Tingart, J. Eschweiler, Role of Implants Surface Modification in Osseointegration: A Systematic Review, J. Biomed. Mater. Res. - Part A. (2019) 1–15. https://doi.org/10.1002/jbm.a.36829.

[22] J.C.M. Souza, M.B. Sordi, M. Kanazawa, S. Ravindran, B. Henriques, F.S. Silva, C. Aparicio, L.F. Cooper, Nano-Scale Modification of Titanium Implant Surfaces to Enhance Osseointegration, Acta Biomater. 94 (2019) 112–131. https://doi.org/10.1016/j.actbio.2019.05.045.

[23] J. A.N. Oliver, Y. Su, X. Lu, P.H. Kuo, J. Du, D. Zhu, Bioactive Glass Coatings on Metallic Implants for Biomedical Applications, Bioact. Mater. 4 (2019) 261–270. https://doi.org/10.1016/j.bioactmat.2019.09.002.

[24] F. Baino, S. Hamzehlou, S. Kargozar, Bioactive Glasses: Where Are We and Where Are We Going?, J. Funct. Biomater. 9 (2018) 25. https://doi.org/10.3390/jfb9010025.

[25] L.L. Hench, The Story of Bioglass®, J. Mater. Sci. Mater. Med. 17 (2006) 967–978. https://doi.org/10.1007/s10856-006-0432-z.

[26] J.R. Jones, Reprint of: Review of Bioactive Glass: From Hench to Hybrids, Acta Biomater. 23 (2015) S53–S82. https://doi.org/10.1016/j.actbio.2015.07.019.

[27] A. Tavakolizadeh, M. Ahmadian, M.H. Fathi, A. Doostmohammadi, E. Seyedjafari, A. Ardeshirylajimi, Investigation of Osteoinductive Effects of Different Compositions of Bioactive Glass Nanoparticles for Bone Tissue Engineering, ASAIO J. 63 (2017) 512–517. https://doi.org/10.1097/MAT.0000000000000509.

[28] B. Lei, X. Chen, Y. Wang, N. Zhao, C. Du, L. Fang, Surface Nanoscale Patterning of Bioactive Glass to Support Cellular Growth and Differentiation, J. Biomed. Mater. Res. Part A. 94A (2010) 1091–1099. https://doi.org/10.1002/jbm.a.32776.

[29] J.I. Rosales-Leal, M.A. Rodríguez-Valverde, G. Mazzaglia, P.J. Ramón-Torregrosa, L. Díaz-Rodríguez, O. García-Martínez, M. Vallecillo-Capilla, C. Ruiz, M.A. Cabrerizo-Vílchez, Effect of Roughness, Wettability and Morphology of Engineered Titanium Surfaces on Osteoblast-Like Cell Adhesion, Colloids Surfaces A Physicochem. Eng. Asp. 365 (2010) 222–229. https://doi.org/10.1016/j.colsurfa.2009.12.017.

[30] D. Bellucci, V. Cannillo, A. Sola, Coefficient of Thermal Expansion of Bioactive Glasses: Available Literature Data and Analytical Equation Estimates, Ceram. Int. 37 (2011) 2963–2972. https://doi.org/10.1016/j.ceramint.2011.05.048.

[31] M.N. Rahaman, D.E. Day, B. Sonny Bal, Q. Fu, S.B. Jung, L.F. Bonewald, A.P. Tomsia, Bioactive Glass in Tissue Engineering, Acta Biomater. 7 (2011) 2355–2373. https://doi.org/10.1016/j.actbio.2011.03.016.

[32] Y. Torres, P. Trueba, J. Pavón, I. Montealegre, J.A. Rodríguez-Ortiz, Designing, Processing and Characterisation of Titanium Cylinders with Graded Porosity: An Alternative to Stress-Shielding Solutions, Mater. Des. 63 (2014) 316–324.

https://doi.org/10.1016/j.matdes.2014.06.012.

[33] H. Eckert, Structural Characterization of Bioactive Glasses by Solid State NMR, J. Sol-Gel Sci. Technol. 88 (2018) 263–295. https://doi.org/10.1007/s10971-018-4795-7.

[34] P. Balasubramanian, A.J. Salinas, S. Sanchez-Salcedo, R. Detsch, M. Vallet-Regi, A.R. Boccaccini, Induction of VEGF Secretion from Bone Marrow Stromal Cell Line (ST-2) by the Dissolution Products of Mesoporous Silica Glass Particles Containing CuO and SrO, J. Non. Cryst. Solids. 500 (2018) 217–224. https://doi.org/10.1016/j.jnoncrysol.2018.07.073.

[35] Y. Torres, S. Lascano, J. Bris, J. Pavón, J.A. Rodriguez, Development of Porous Titanium for Biomedical Applications: A Comparison between Loose Sintering and Space-Holder Techniques, Mater. Sci. Eng. C. 37 (2014) 148–155. https://doi.org/10.1016/j.msec.2013.11.036.

[36] S. Lascano, C. Arévalo, I. Montealegre-Melendez, S. Muñoz, J.A. Rodriguez-Ortiz, P. Trueba, Y. Torres, Porous Titanium for Biomedical Applications: Evaluation of the Conventional Powder Metallurgy Frontier and Space-Holder Technique, Appl. Sci. 9 (2019). https://doi.org/10.3390/app9050982.

[37] C. Domínguez-Trujillo, F. Ternero, J.A. Rodríguez-Ortiz, S. Heise, A.R. Boccaccini, J. Lebrato, Y. Torres, Bioactive Coatings on Porous Titanium for Biomedical Applications, Surf. Coatings Technol. 349 (2018) 584–592. https://doi.org/10.1016/j.surfcoat.2018.06.037.

[38] C. Domínguez-Trujillo, F. Ternero, J.A. Rodríguez-Ortiz, J.J. Pavón, I. Montealegre-Meléndez, C. Arévalo, F. García-Moreno, Y. Torres, Improvement of the Balance between a Reduced Stress Shielding and Bone Ingrowth by Bioactive Coatings onto Porous Titanium Substrates, Surf. Coatings Technol. 338 (2018) 32–37. https://doi.org/10.1016/j.surfcoat.2018.01.019.

[39] T. Kokubo, H. Takadama, How Useful is SBF in Predicting In Vivo Bone Bioactivity?, Biomaterials. 27 (2006) 2907–2915. https://doi.org/10.1016/j.biomaterials.2006.01.017.

[40] M.W.G. Lockyer, D. Holland, R. Dupree, NMR Investigation of the Structure of Some Bioactive and Related Glasses, J. Non. Cryst. Solids. 188 (1995) 207–219. https://doi.org/10.1016/0022-3093(95)00188-3.

[41] V. FitzGerald, D.M. Pickup, D. Greenspan, G. Sarkar, J.J. Fitzgerald, K.M. Wetherall, R.M. Moss, J.R. Jones, R.J. Newport, A Neutron and X-Ray Diffraction Study of Bioglass® with Reverse Monte Carlo Modelling, Adv. Funct. Mater. 17 (2007) 3746–3753. https://doi.org/10.1002/adfm.200700433.

[42] P. Trueba, A.M. Beltrán, J.M. Bayo, J.A. Rodríguez-ortiz, D.F. Larios, E. Alonso, D.C. Dunand, Y. Torres, Porous titanium Cylinders Obtained by the Freeze- Casting Technique: Influence of Process Parameters on Porosity and Mechanical Behavior, Metals 10 (2020) 188. https://doi.org/10.3390/met10020188.

[43] Standard Test Method for ASTM C373-14, Standard Test Method for Water Absorption, Bulk Density, Apparent Porosity, and Apparent Specific Gravity of Fired Whiteware Products, Ceramic Tiles, and Glass Tiles, West Conshohocken, PA, 2014. https://doi.org/10.1520/C0373-14.

[44] R.I.M. Asri, W.S.W. Harun, M.A. Hassan, S.A.C. Ghani, Z. Buyong, A Review of Hydroxyapatite-Based Coating Techniques: Sol-Gel and Electrochemical Depositions on Biocompatible Metals, J. Mech. Behav. Biomed. Mater. 57 (2016) 95–108. https://doi.org/10.1016/j.jmbbm.2015.11.031.

[45] F. Abushahba, E. Söderling, L. Aalto-Setälä, J. Sangder, L. Hupa, T.O. Närhi, Antibacterial Properties of Bioactive Glass Particle Abraded Titanium Against Streptococcus Mutans, Biomed. Phys. Eng. Express. 4 (2018) 45002.

https://doi.org/10.1088/2057-1976/aabeee.

[46] C.M. Botelho, R.A. Brooks, S.M. Best, M.A. Lopes, J.D. Santos, N. Rushton, W. Bonfield, Human Osteoblast Response to Silicon-Substituted Hydroxyapatite, J. Biomed. Mater. Res. Part A. 79A (2006) 723–730. https://doi.org/10.1002/jbm.a.30806.

[47] D.C. Clupper, L.L. Hench, Crystallization Kinetics of Tape Cast Bioactive Glass 45S5, J. Non. Cryst. Solids. 318 (2003) 43–48. https://doi.org/10.1016/S0022-3093(02)01857-4.

[48] Q.Z. Chen, I.D. Thompson, A.R. Boccaccini, 45S5 Bioglass®-Derived Glass-Ceramic Scaffolds for Bone Tissue Engineering, Biomaterials. 27 (2006) 2414–2425. https://doi.org/10.1016/j.biomaterials.2005.11.025.

[49] A.S. Bakry, Y. Tamura, M. Otsuki, S. Kasugai, K. Ohya, J. Tagami, Cytotoxicity of 45S5 Bioglass Paste Used for Dentine Hypersensitivity Treatment, J. Dent. 39 (2011) 599–603. https://doi.org/10.1016/j.jdent.2011.06.003.

[50] M.C. Crovace, M.T. Souza, C.R. Chinaglia, O. Peitl, E.D. Zanotto, Biosilicate® - A Multipurpose, Highly Bioactive Glass-Ceramic. In Vitro, In Vivo and Clinical Trials, J. Non. Cryst. Solids. 432 (2016) 90–110. https://doi.org/10.1016/j.jnoncrysol.2015.03.022.

[51] F.E. Ciraldo, E. Boccardi, V. Melli, F. Westhauser, A.R. Boccaccini, Tackling Bioactive Glass Excessive In Vitro Bioreactivity: Preconditioning Approaches for Cell Culture Tests, Acta Biomater. 75 (2018) 3–10. https://doi.org/10.1016/j.actbio.2018.05.019.

Table of content

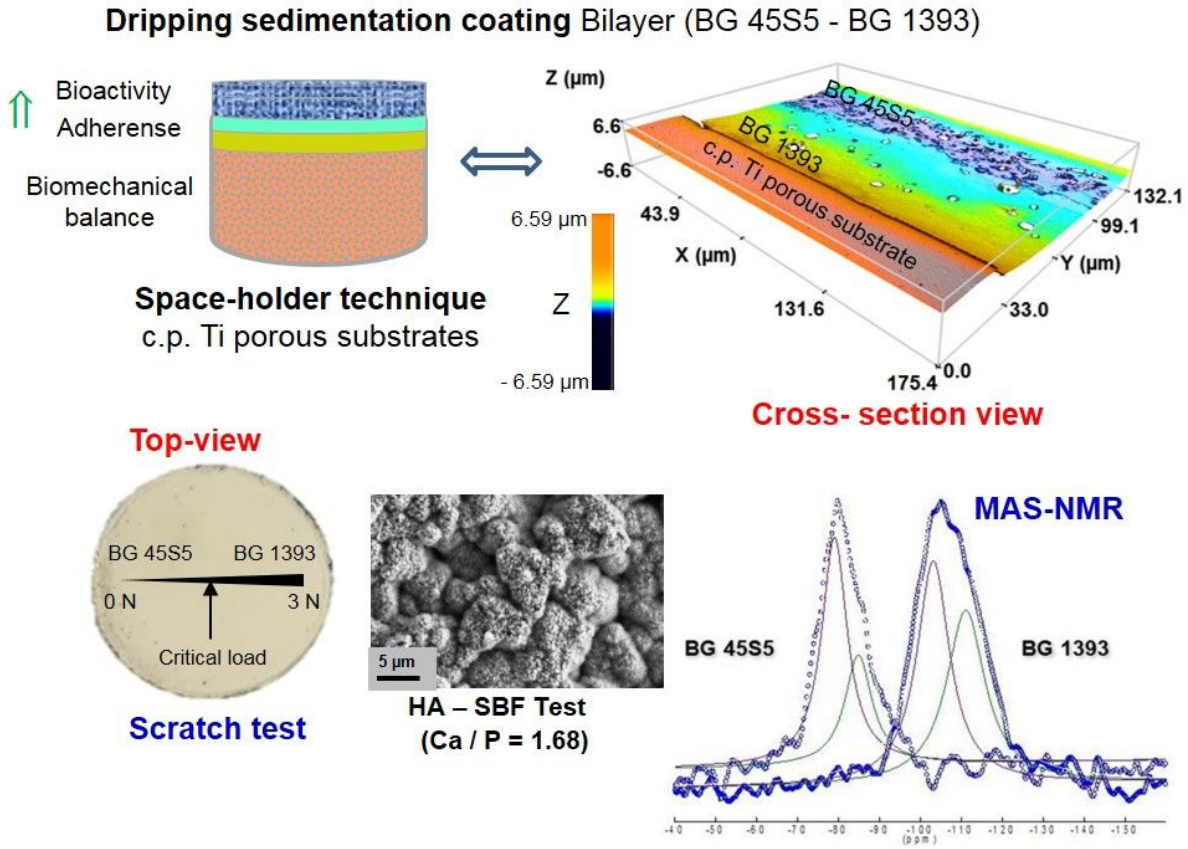

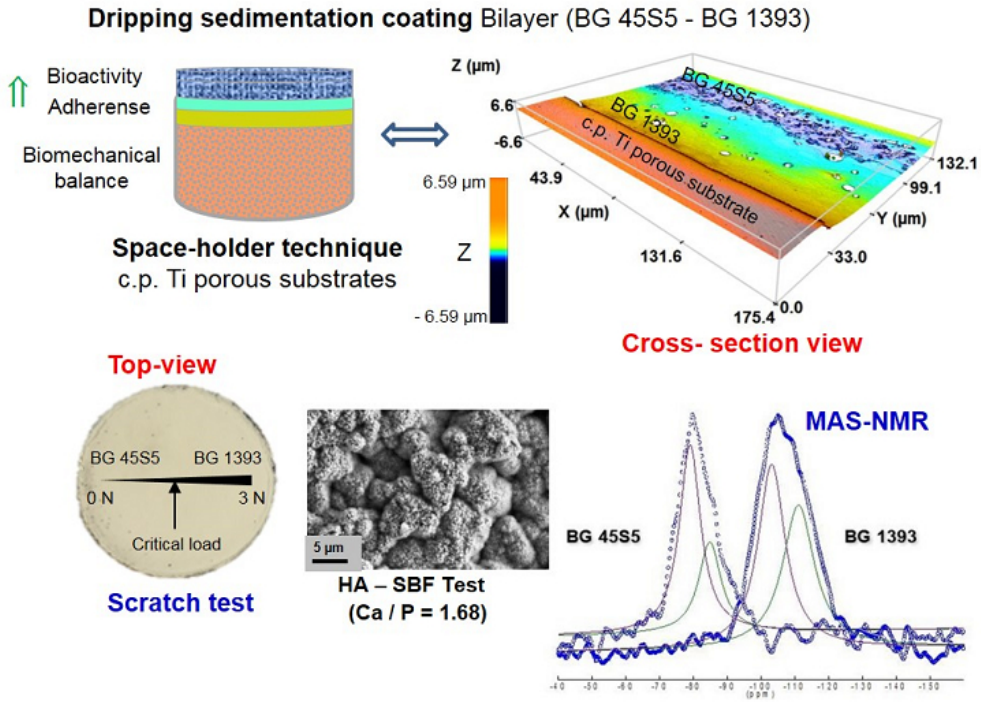
Dripping sedimentation coating Bilayer (BG 45S5 - BG 1393)
Bioactivity
Adherense
Biomechanical balance
Space-holder technique
c.p. Ti porous substrates
Z (µm)
6.6
-6.6
6.59 µm
Z
- 6.59 µm
BG 45S5
BG 1393
c.p. Ti porous substrate
43.9
X (µm)
131.6
132.1
99.1
Y (µm)
33.0
175.4
0.0
Cross- section view
Top-view
BG 45S5
BG 1393
0 N
3 N
Critical load
Scratch test
5 µm
HA – SBF Test
(Ca / P = 1.68)
MAS-NMR
BG 45S5
BG 1393